Electronic Absorption, Resonance Raman, and Electrochemical Studies of Planar and Saddled Copper(III) *meso*-Triarylcorroles. Highly Substituent-Sensitive Soret Bands as a Distinctive Feature of High-Valent Transition Metal Corroles

Ingar H. Wasbotten, Tebikie Wondimagegn, and Abhik Ghosh*

Contribution from the Department of Chemistry, University of Tromsø, N-9037 Tromsø, Norway

Received June 4, 2001

Abstract: We present here a first systematic study of substituent effects in metallocorroles, based on electronic absorption, resonance Raman (RR), and infrared (IR) spectroscopic studies and electrochemical measurements on 10 copper(III) *meso*-triarylcorroles, $Cu^{III}[\beta-Y_8TArC]$, where the β-substituent Y = H or Br and the *meso*-aryl group Ar = C_6F_5 or p-X-C_6H_4 and X = CF_3, H, CH_3, and OCH_3. The results afford a number of significant inisights. (1) The RR (and IR) results show that at least two and possibly more high-frequency bands in the $1400-1550$ cm^{-1} region exhibit significant frequency downshifts on β-octabromination and, thus, qualify as structure-sensitive marker bands. DFT geometry optimizations indicate that the saddled conformation should be clearly preferred for the β-octabromo-*meso*-triarylcorrole derivatives studied and that β-octabromination results in expansion of a number of skeletal bond distances of the corrole macrocycle, consistent with observed frequency downshifts. (2) Electrochemical measurements on planar $Cu^{III}[TArC]$ derivatives have shown that the para substituents on the *meso*-aryl groups exert a strong influence on the half-wave potentials for oxidation ($\rho_{ox} = \Delta E_{1/2ox}/\Delta(3\sigma) = 95$ mV), suggesting that oxidation involves removal of an electron from the corrole "b_1" HOMO, which has significant amplitudes at the meso postions and crudely resembles a porphyrin a_{2u} HOMO in shape. In contrast, the Hammett ρ_{ox} is much lower for the nonplanar $Cu^{III}[Br_8TArC]$ derivatives and we suggest that this ultimately results from a b_1-to-a_2 HOMO reversal which in turn stems from a metal ($d_{x^2-y^2}$)$-$corrole ("b_1") orbital interaction that becomes symmetry-allowed under a saddle distortion of the corrole macrocycle. In contrast to what has been observed for metallotetraphenylporphyrins, β-octabromination dramatically raises the half-wave potential for one-electron oxidation of the triarylcorrole derivatives studied. This appears to be due to the fact that both the "a_2" and "b_1" HOMOs of a corrole (in C_{2v} notation) have significantly higher amplitudes at the β positions, compared to a porphyrin a_{2u} HOMO. Thus, although many metallocorroles are significantly more easily oxidizable than analogous metalloporphyrins, certain β-octahalogeno-*meso*-triarylcorrole derivatives can indeed be extremely electron deficient and oxidation resistant and may, therefore, find use as rugged catalysts or reagents under highly oxidizing conditions. (3) Finally, the Soret absorption maxima of high-valent metallotriarylcorroles exhibit a uniquely sensitive dependence on the substituents on the *meso*-aryl groups. Thus, on going from $Cu^{III}[T(p-CF_3-P)C]$ (T(p-CF$_3$-P)C = *meso*-tris((p-trifluoromethyl)phenyl)corrolato) to $Cu^{III}[T(p-OM-P)C]$ (T(p-OM-P)C = *meso*-tris(p-methoxyphenyl)corrolato), the Soret maximum red shifts by 26 nm, from 407 to 433 nm. Similarly, on going from $Cu^{III}[Br_8T(p-CF_3-P)C]$ (Br$_8$T(p-CF$_3$-P)C = β-octabromo-*meso*-tris((p-trifluoromethyl)phenyl)corrolato) to $Cu^{III}[Br_8T(p-OM-P)C]$ (Br$_8$T(p-CF$_3$-P)C = β-octabromo-*meso*-tris(p-methoxyphenyl)corrolato), the Soret maximum red shifts by 34 nm, from 434 to 468 nm. Time-dependent DFT calculations suggest that this substituent dependence reflects significant ligand-to-metal charge-transfer character of certain transitions in the Soret region. The optical spectra of free-base and non-high-valent transition metal tetrapyrroles, in general, do not exhibit a similar substituent dependence.
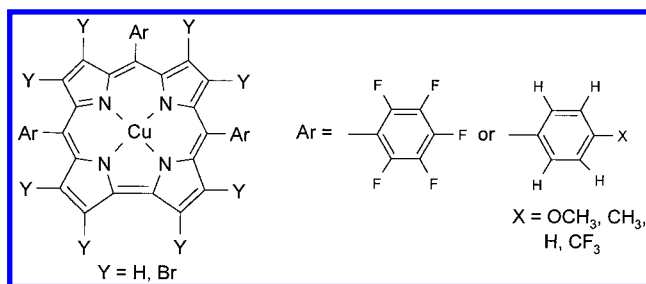
Introduction

The chemistry of corroles and metallocorroles has undergone a remarkable renaissance during the past few years.[1,2] Two developments appear to have contributed to the current high level of interest in these compounds. Vogel[3-5] and co-workers and, subsequently, others[6-9] have shown that the trianionic corrole ligand can stabilize transition metal ions in high oxidation states. Second, Gross and others have reported simple

* Corresponding author. E-mail: abhik@chem.uit.no.

(1) Paolesse, R. In *The Porphyrin Handbook*; Kadish, K. M., Smith, K. M., Guilard, R., Eds.; Academic: San Diego, CA, 2000; Vol. 2, Chapter 11, p 201.

(2) Erben, C.; Will, S.; Kadish, K. M. In *The Porphyrin Handbook*; Kadish, K. M., Smith, K. M., Guilard, R., Eds.; Academic: San Diego, CA, 2000; Vol. 2, Chapter 12, p 233.

(3) Vogel, E.; Will, S.; Schulze Tilling, A.; Neumann, L.; Lex, J.; Bill, E.; Trautwein, A. X.; Wieghardt, K. *Angew. Chem., Int. Ed. Engl.* **1994**, *33*, 731; *Angew. Chem.* **1994**, *106*, 771.

(4) Will, S.; Lex, J.; Vogel, E.; Schmickler, H.; Gisselbrecht, J.-P.; Haubtmann, C.; Bernard, M.; Gross, M. *Angew. Chem., Int. Ed. Engl.* **1197**, *36*, 357.
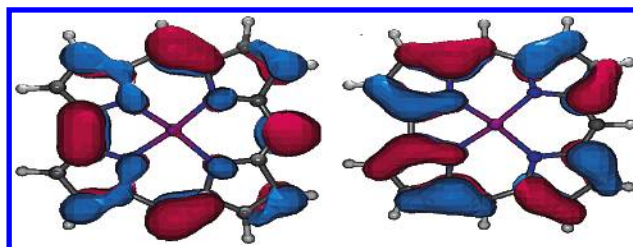
Figure 1. Cu(III) *meso*-triarylcorroles studied in this work.

Figure 2. The b_1 and a_2 HOMOs of Ga(III) corrole, chosen as a representative closed-shell metallocorrole.[24]

one-pot syntheses of free-base corroles,[10,11] which were previously accessible only via much longer multistep routes. These developments have stimulated considerable progress in the coordination chemistry of corroles and a wide variety of transition metal corroles have been synthesized and characterized.[1–9] However, outside of our own work,[12] there has been relatively little study of the effect of peripheral substituents on metallocorroles.[13] Against this background, we present here a first major exploration of this topic. The results we present consist of resonance Raman, infrared, and electronic absorption spectroscopic and electrochemical measurements on 10 new copper(III) triarylcorroles, $Cu^{III}[\beta-Y_8TArC]$ (where the β-substituent Y = H or Br and the *meso*-aryl group Ar = C_6F_5 or p-X-C_6H_4 and X = CF_3, H, CH_3, and OCH_3; Figure 1), along with supporting DFT calculations. Measurements of substituent effects often turn out to be much more than an end in themselves, with substituent effects serving as unique probes of mechanistic and electronic-structural issues. Gratifyingly, this is also what happened in this study. Thus, the various measurements described here significantly enhance our understanding of the electronic and geometric effects of nonplanar distortions in porphyrin-type molecules, a subject of considerable current interest. Another highlight of this study is the novel observation that Cu(III) and other high-valent transition metal corroles[13] exhibit intense, exquisitely substituent-sensitive absorptions in the Soret region. This feature appears to be specific for high-valent complexes and is not shared by (or, at least, is not readily observable for) free-base and non-high-valent transition metal tetrapyrroles.

The specific issues that we have addressed in this study are as follows.

(1) The high-frequency (1000–1650 cm^{-1}) skeletal vibrations of metalloporphyrins are a rich source of information on many

detailed aspects of the structures of these molecules.[14] Thus, the frequencies of these "marker bands" can furnish information on such issues as (i) the core size of the metalloporphyrin,[15–17] (ii) the degree of saddling or ruffling in the case of nonplanar porphyrins,[18–21] and (iii) whether the porphyrin[22,23] ligand is innocent or has radical character. Our recent theoretical studies[24] on corroles suggested that the high-frequency skeletal vibrations of corroles[2,25] should be equally informative. Having gained access to two analogous series of planar and nonplanar corroles (Figure 1), we have investigated whether corroles, like porphyrins, also exhibit structure-sensitive marker bands, i.e., whether the resonance Raman (and infrared) spectra of corroles exhibit readily identifiable features that are indicative of structural and/ or electronic perturbations.

(2) The electrochemical half-wave potentials for one-electron oxidation of many metallocorroles are significantly lower (by a few hundred millivolts) than those of the analogous metalloporphyrins.[2,26] For example, the half-wave potential for one-electron oxidation of Sn(OEC)Cl is 0.67 V compared to 1.36 V for Sn(OEP)Cl$_2$ (OEC = β-octaethylcorrole and OEP = β-octaethylporphyrin; potentials vs the saturated calomel electrode).[2] Accordingly, from the point of view of substituent effects, an important issue involves whether suitably substituted electron-deficient metallocorroles can serve as stable catalysts or reagents under highly oxidizing reaction conditions. Based on reactivity studies by Gray, Goldberg, and Gross and co-workers[27] and our electrochemical measurements, we shall see that the answer to this question appears to be "yes".

Because the corrole a_2 and b_1 HOMOs are relatively similar in shape to the a_{1u} and a_{2u} HOMOs of porphyrins (Figure 2),[24]

(5) Van Caemelbecke, E.; Will, S.; Autret, M.; Adamian, V. A.; Lex, J.; Gisselbrecht, J.-P.; Gross, M.; Vogel, E.; Kadish, K. M. *Inorg Chem.* **1996**, *35*, 184.
(6) Gross, Z.; Golubkov, G.; Simkhovich, L. *Angew. Chem., Int. Ed. Engl.* **2000**, *39*, 4045.
(7) Simkhovich, L.; Galili, N.; Saltsman, I.; Goldberg, I.; Gross, Z. *Inorg. Chem.* **2000**, *39*, 2704.
(8) Meier-Callahan, A. E.; Gray, H. B.; Gross, Z. *Inorg. Chem.* **2000**, *39*, 3605.
(9) Cai, S.; Walker, F. A.; Licoccia, S. *Inorg. Chem.* **2000**, *39*, 3466.
(10) Gross, Z.; Galili, N.; Saltsman, I. *Angew. Chem. Int. Ed.* **1999**, *38*, 1427.
(11) Gross, Z.; Galili, N.; Simkhovich, L.; Saltsman, I.; Botoshansky, M.; Bläser, D.; Boese, R.; Goldberg, I. *Org. Lett.* **1999**, *1*, 599.
(12) Steene, E.; Wondimagegn, T.; Ghosh, A. *J. Phys. Chem. B* **2001**, *105*, 11406. For an Addition/Correction, see: *J. Phys. Chem. B* **2002**, *106*, 5312.
(13) To our knowledge, Boschi, Kadish, and co-workers (Adamian, V. A.; D'Souza, F.; Licoccia, S.; Di Vona, M. L.; Tassoni, E.; Paolesse, R.; Boschi, T.; Kadish, K. M. *Inorg. Chem.* **1995**, *34*, 532) were the first to report an electrochemical study of substituent effects in corrole derivatives. They examined the electrochemical behavior of (5,10,15-tri-X-phenyl,2,3,7,8,-12,13,17,18-octamethylcorrolato)cobalt(III) triphenylphosphine, where X = *p*-OCH$_3$, *p*-CH$_3$, *p*-Cl, *m*-Cl, *o*-Cl, *m*-F, *o*-F, or H), and detected significant substituent effects on the redox potentials. However, as we shall discuss later in the paper, the Soret absorption maxima of these non-high-valent Co(III) complexes did not vary significantly as a function of the meso substituents.
(14) Procyk, A. D.; Bocian, D. F. *Annu. Rev. Phys. Chem.* **1992**, *43*, 465.
(15) Spaulding, L. D.; Chang, C. C.; Yu, N.-T.; Felton, R. H. *J. Am. Chem. Soc.* **1975**, *97*, 2517.
(16) Stong, J. D.; Kubaske, R. J.; Shupack, S. I.; Spiro, T. G. *J. Raman Spectrosc.* **1980**, *9*, 312.
(17) Parthasarathi, N.; Hansen, C.; Yamaguchi, S.; Spiro, T. G. *J. Am. Chem. Soc.* **1987**, *109*, 3865.
(18) Shelnutt, J. A.; Medforth, C. J.; Berber, M. D.; Barkigia, K. M.; Smith, K. M. *J. Am. Chem. Soc.* **1991**, *113*, 4077.
(19) Sparks, L. D.; Anderson, K. K.; Medforth, C. J.; Smith, K. M.; Shelnutt, J. A. *Inorg. Chem.* **1994**, *33*, 2297.
(20) Jentzen, W.; Simpson, M. C.; Hobbs, J. D.; Song, X.; Ema, T.; Nelson, N. Y.; Medforth, C. J.; Smith, K. M.; Veyrat, M.; Mazzanti, M.; Ramasseul, R.; Marchon, J.-C.; Takeuchi, T.; Goddard, W. A., III; Shelnutt, J. A. *J. Am. Chem. Soc.* **1995**, *117*, 11085.
(21) For an RR study of β-octahalogeno-*meso*-tetraarylmetalloporphyrins, see: Halvorsen, I.; Steene, E.; Ghosh, A. *J. Porphyrins Phthalacyanines* **2001**, *5*, 721.
(22) Czernuzewicz, R. S.; Macor, K. A.; Li, X.-Y.; Kincaid, J. R.; Spiro, T. G. *J. Am. Chem. Soc.* **1990**, *111*, 3860.
(23) Macor, K. A.; Czernuzewicz, R. S.; Spiro, T. G. *Inorg. Chem.* **1990**, *29* 1996.
(24) Ghosh, A.; Wondimagegn, T.; Parusel, A. B. J. *J. Am. Chem. Soc.* **2000**, *122*, 5100.
(25) For a review on corroles, see: Paolesse, R. In *The Porphyrin Handbook*; Kadish, K. M., Smith, K. M., Guilard, R., Eds.; Academic: San Diego, CA, 2000; Vol. 2, Chapter 11, p 201.
(26) Gross, Z. *J. Biol. Inorg. Chem.* **2001**, *7*, 733
(27) Golubkov, G.; Bendix, J.; Gray, H. B.; Mahammed, A.; Goldberg, I.; DiBilio, A. J.; Gross, Z. *Angew. Chem., Int. Ed.* **2001**, *40*, 2132.

respectively, we wished to determine whether known trends in substitutent effects on the half-wave potentials of metalloporphyrins also apply to metallocorroles. We shall see that there are both interesting similarities and differences between metalloporphyrins and metallocorroles with respect to this issue.

(3) A key finding of this study is the unique substituent sensitivity exhibited by the optical spectra of high-valent transition metal corroles. In general, optical spectroscopy is not particularly useful for studies of substituent effects in metalloporphyrins: the Q- and the B-bands typically do not shift significantly within a family of metalloporphyrins with substituents with systematically varying electron donating or withdrawing power. For example, for a series of nickel β-octabromo-*meso*-tetraarylporphyrins with variable para substituents on the phenyl groups, Ni[Br$_8$T(p-X-P)P] (X = CH$_3$, H, F, Br, COOMe, CF$_3$, NO$_2$), the absorption maxima of the B- and Q-bands are 447 ± 3 (Soret), 560 ± 2 (Q), 590 ± 3 nm (Q), respectively.[28] Against this backdrop, we report here that the Soret absorption maxima of high-valent[29] copper(III) corroles are extremely sensitive to the electronic effects of peripheral substituents. We have attempted to explain this observation by means of time-dependent DFT calculations. We believe that the optical spectra of the compounds studied here, along with those of Fe(IV) and Mn(IV) corroles we have described elsewhere,[12] provide some of the "cleanest" examples of substituent effects on LMCT transitions in high-valent transition metal complexes.

Experimental Section

General Comments. Proton NMR spectra were recorded with a JEOL 400 MHz spectrometer at 298 K in CDCl$_3$. UV−vis spectra were recorded with an HP 8453 spectrophotometer in CH$_2$Cl$_2$. Infrared spectra were obtained with a Perkin-Elmer 1600 FTIR instrument using KBr pellets. MALDI-TOF mass spectra were recorded on a Biflex instrument from Bruker Daltonics, Inc. For the MS measurements, the compounds were dissolved in a mixed solvent containing 50% CHCl$_3$, 45% MeOH/2-propanol (7/3), 0.1% TFA, and 5% water and the matrix used was α-cyanohydroxycinnamic acid (α-CHCA). Column chromatography was performed on basic alumina ("activity stage I") from Merck or Matrex Silica 60A/35-70 m from Millipore. Resonance Raman (RR) spectra were obtained with a Spex Jobin-Yvon double monochromator equipped with a liquid nitrogen-cooled Spex Jobin-Yvon CCD 2000 detector and a Coherent Innova 70 Series mixed Ar−Kr laser. The laser line at 457.9 nm was used to obtain Soret-excited RR spectra. RR measurements were carried out on solutions of the metalloporphyrins in dichloromethane placed inside sealed glass capillaries. Sample integrity was monitored by UV−visible absorption spectroscopy immediately before and after the RR spectra were obtained. No sample photodegradation was apparent as a result of the laser irradiation. Cyclic voltammetry was carried out using an EG&G Model 263A Potentiostat with a three-electrode system consisting of a glassy carbon working electrode, a platinum wire counter electrode, and a saturated calomel reference electrode (SCE). Tetra(*n*-butyl)-ammonium perchlorate (TBAP), recrystallized from ethanol and dried in a desiccator for at least one week, was used as the supporting electrolyte. Dichloromethane, distilled and stored over molecular sieves, was used as the solvent for the cyclic voltammetry experiments. The reference electrode was separated from the bulk solution by a fritted-glass bridge filled with the solvent/supporting electrolyte mixture and all redox potentials reported here are referenced to the SCE. Pure argon

was bubbled through solutions containing the metallocorroles for at least 2 min prior to the cyclic voltammetry experiments and the solutions were also protected from air by an argon blanket during the experiment.

General Synthesis of Free-Base *meso*-Triarylcorroles. A 1.5 g sample of basic alumina (with the exception of *meso*-triphenylcorrole, for which neutral alumina resulted in somewhat better yields) was placed in a 50 mL round-bottomed flask with a stirring bar, distilled pyrrole (9.68 mmol), an aromatic aldehyde (9.68 mmol), and 1 mL of CH$_2$Cl$_2$. The flask was slowly heated to 70 °C and maintained at this temperature for 4 h. Heating was then discontinued, 50−70 mL of CH$_2$-Cl$_2$ was added, the solids were dislodged from the walls of the flask with a spatula, the mixture was swirled, and the solids were brought into solution as quickly and as much as possible. The mixture was then suction-filtered with a Büchner funnel. DDQ (4.84 mmol) was then added to the filtrate and the mixture was stirred for an hour. The mixture was then filtered again with the aid of a Büchner funnel. The filtrate was evaporated to dryness and the dry material was subjected to flash chromatography. The stationary and mobile phases used, which varied somewhat for the different corroles synthesized, are indicated below. The first fraction to elute generally consisted of the tetraarylporphyrin. The corrole followed next and it was best identified by its UV−visible spectrum. All the free-base *meso*-triarylcorroles prepared are strongly fluorescent.

Flash chromatography of 5,10,15-tris(pentafluorophenyl)corrole, H$_3$TPFPC: Basic alumina and CH$_2$Cl$_2$/hexane (1:1). Yield: 6−10%.

Flash chromatography of 5,10,15-tris(*p*-trifluouromethylphenyl)-corrole, H$_3$T(*p*-CF$_3$-P)C: Basic alumina and CH$_2$Cl$_2$/hexane (1:1). Yield: 7−10%.

Flash chromatography of 5,10,15-tris(*p*-methylphenyl)corrole, H$_3$T(*p*-CH$_3$-P)C: Silica and pentane/CH$_2$Cl$_2$ (3:2). Yield: 6−7%.

Flash chromatography of 5,10,15-triphenylcorrole, H$_3$TPC: Silica and hexane/CH$_2$Cl$_2$ (1:1). Yield: 6−7%.

Flash chromatography of 5,10,15-tri(*p*-methoxyphenyl)corrole, H$_3$T(*p*-OCH$_3$-P)C: Silica and CH$_2$Cl$_2$/pentane (5:1). Yield: 2−5%.

Synthesis of Cu(III) Triarylcorroles: The free-base triarylcorrole (0.040 g) was dissolved in 25 mL of pyridine at room temperature, 0.040 g of Cu(OAc)$_2$·4H$_2$O was added, and the mixture was stirred for 15 min. The pyridine was removed via vacuum distillation and the product was obtained by flash chromatography of the residue on silica gel with CH$_2$Cl$_2$ (for Cu[TPFPC]) or 2:1 hexane/CH$_2$Cl$_2$ (for the other compounds) as eluent.

Synthesis of Cu(III) β-Octabromo-*meso*-triarylcorroles. To a stirred solution of the Cu(III) triarylcorrole (0.075 mmol) in 20 mL of CHCl$_3$ was added 2.25 mmol of liquid bromine, dissolved in 8 mL of CHCl$_3$, over a period of 15 min at room temperature. After the mixture was stirred for 1 h, pyridine (2.70 mmol), dissolved in 8 mL of CHCl$_3$, was added dropwise over a period of 15 min and the solution was then stirred for a period of 1 h. The reaction mixture was shaken with 15 mL of 20% (w/v) aqueous sodium metabisulfite. The organic layer was separated and dried with anhydrous sodium sulfate. The solvent was rotary evaporated and the product was obtained by flash chromatography of the residue on a silica gel column with CH$_2$Cl$_2$ (for CuBr$_8$-TPFPC) or hexane/CH$_2$Cl$_2$ (1:1) (for the other derivatives) as eluent.

All compounds were characterized by optical spectroscopy, ^{1}H NMR and 2D COSY, resonance Raman and infrared spectroscopies, MALDI-TOF mass spectrometry, and elemental analyses. Complete spectroscopic characterization of the following compounds has been reported elsewhere: H$_3$T(*p*-OCH$_3$-P)C,[30] H$_3$T(*p*-CH$_3$-P)C,[30] H$_3$TPC,[30] and H$_3$-TPFPC.[10] The following describes the characterization of the compounds that are reported here for the first time. The ^{1}H NMR and IR spectra of the new compounds reported are also included as Supporting Information.

(28) Ghosh, A.; Halvorsen, I.; Steene, E.; Nilsen, H. J.; Lie, R.; Van Caemelbecke, E.; Guo, N.; Ou, Z.; Kadish, K. M. *J. Phys. Chem. B* **2001**, *105*, 8120.

(29) For a series of edited review articles on high-valent metalloporphyrins and related compounds, see: Ghosh, A. *J. Biol. Inorg. Chem.* **2001**, *7*, 726.

(30) Paolesse, R.; Nardis, S.; Sagone, F.; Khoury, R. G. *J. Org. Chem.* **2001**, *66*, 550.

H₃[T(*p*-CF₃-P)C]. UV−vis: λ_{max} 417 (log ϵ = 4.86), 576 (log ϵ = 4.11), 615 (log ϵ = 3.94), 646 nm (log ϵ = 3.81). ¹H NMR (CDCl₃): δ 8.94−8.96 (m, 4H), 8.64 (s, 2H), 8.46−8.51 (m, 6H), 8.15 (d, *J* = 7.0 Hz, 4H), 7.67 (d, *J* = 8.2 Hz, 2 H), 7.59 (d, *J* = 8.6 Hz, 2H), 2.44 (s, 3H). MS (MALDI-TOF): 730.24 (M⁺); calcd 730.64. IR ν_{max}/cm⁻¹: 2923, 2855, 2368, 1929, 1705, 1612, 1566, 1512, 1458, 1404, 1327, 1165, 1126, 1065, 1018, 948, 856, 802, 741, 856, 802, 741, 710, 602.

Cuᴵᴵᴵ[TPC]. ¹H NMR: δ 7.89 (broad singlet, 2H, β-pyrrolic), 7.76 (d, *J* = 7.3 Hz, 4H, *m*- or *o*-phenyl), 7.65 (d, *J* = 7.3 Hz, 4 H, β-pyrrolic and *o*-phenyl), 7.54−7.59 (m, 3H, *p*-phenyl), 7.44−7.51 (m, 6H, *m*- or *o*-phenyl), 7.35 (d, *J* = 3.1 Hz, 2H, β-pyrrolic), 7.24 (2H, β-pyrrolic). UV−vis: λ_{max} (log ϵ/(M⁻¹ cm⁻¹)) 410 (5.09), 538 nm (3.89). MS (MALDI-TOF): 586.96 (M⁺); calcd 587.16. IR ν_{max}/cm⁻¹: 3098, 3049, 2923, 2360, 2342, 1959, 1596, 1514, 1491, 1438, 1423, 1363, 1340, 1309, 1263, 1247, 1224, 1190, 1155, 1068, 1053, 1027, 1019, 980, 923, 893, 870, 841, 822, 789, 771, 756, 711, 698, 669, 654, 619.

Cuᴵᴵᴵ [T(*p*-CF₃-P)C]. ¹H NMR: δ 7.90 (d, *J* = 3.1 Hz, 2H, β-pyrrolic), 7.83 (d, *J* = 7.9 Hz, 4H, *m*- or *o*-phenyl), 7.76 (d, *J* = 8.6, 5H, *m*- or *o*-phenyl), 7.72 (d, *J* = 3.05 Hz, 3H, *m*- or *o*-phenyl), 7.56 (d, *J* = 4.3 Hz, 2H, β-pyrrolic), 7.29 (d, *J* = 4.3 Hz, 2H, β-pyrrolic), 7.17 (d, *J* = 4.9 Hz, 2H, β-pyrrolic). UV−vis: λ_{max} (log ϵ/(M⁻¹ cm⁻¹)) 407 nm (4.94). MS (MALDI-TOF): 730.24 (M⁺); calcd 730.64. IR ν_{max}/cm⁻¹: 2924, 2855, 2361, 1612, 1520, 1404, 1327, 1165, 1126, 1065, 1018, 980, 864, 826, 787, 710, 671, 610.

Cuᴵᴵᴵ[T(*p*-OCH₃-P)C]. ¹H NMR: δ 7.92 (broad singlet, 2H, β-pyrrolic), 7.74 (d, *J* = 8.6 Hz, 6H, β-pyrrolic and *m*- or *o*-phenyl), 7.65 (d, *J* = 8.6 Hz, 2H, *m*- or *o*-phenyl), 7.41 (s, 2H, β-pyrrolic), 7.34 (d, *J* = 3.7 Hz, 2H, β-pyrrolic), 7.02 (d, *J* = 7.9 Hz, 4H, *m*- or *o*-phenyl), 6.99 (d, *J* = 8.6 Hz, 2H, *m*- or *o*-phenyl), 3.92 (s, 6H, *p*-OCH₃), 3.91 (s, 3H, *p*-OCH₃). UV−vis: λ_{max} (log ϵ/(M⁻¹ cm⁻¹)) 433 nm (4.93). MS (MALDI-TOF): 677.12 (M⁺); calcd 677.24. IR ν_{max}/cm⁻¹: 2993, 2951, 2928, 2831, 2359, 2342, 1601, 1570, 1506, 1463, 1437, 1424, 1364, 1340, 1300, 1250, 1173, 1109, 1053, 1021, 980, 872, 821, 788, 768, 730, 708, 668, 610.

Cuᴵᴵᴵ[T(*p*-CH₃-P)C]. ¹H NMR: δ 7.86 (s, 2H, β-pyrrolic), 7.66 (d, *J* = 7.8 Hz, 6H, β-pyrrolic and *m*- or *o*-phenyl), 7.56 (d, *J* = 7.8 Hz, 2H, *m*- or *o*-phenyl), 7.36 (d, *J* = 4.1 Hz, 2H, β-pyrrolic), 7.29 (d, *J* = 7.6 Hz, 4H, *m*- or *o*-phenyl), 7.27 (d, *J* = 3.4 Hz, 2H, *m*- or *o*-phenyl), 7.25 (s, 2H, β-pyrrolic), 2.43 (s, 6H, *p*-CH₃), 2.41 (s, 3H, *p*-CH₃). UV−vis: λ_{max} (log ϵ/(M⁻¹ cm⁻¹)): 418 nm (4.97). MS (MALDI-TOF): 628.00 (M⁺); calcd 629.24. IR ν_{max}/cm⁻¹: 3020, 2918, 2860, 2361, 2343, 1605, 1560, 1506, 1486, 1442, 1424, 1401, 1363, 1340, 1248, 1224, 1181, 1109, 1053, 1040, 1028, 1017, 980, 894, 871, 852, 838, 806, 788, 768, 724, 706, 668, 640, 606.

Cuᴵᴵᴵ[TPFPC]. ¹H NMR: δ 7.97 (d, *J* = 4.9 Hz, 2H, β-pyrrolic), 7.38 (d, *J* = 4.9 Hz, 2H, β-pyrrolic), 7.19 (d, *J* = 4.9 Hz, 2H, β-pyrrolic), 7.02 (d, *J* = 4.9 Hz, 2H, β-pyrrolic). UV−vis: λ_{max} (log ϵ/(M⁻¹ cm⁻¹)) 406 nm (4.79). MS (MALDI-TOF): 856.88 (M⁺); calcd 857.02. IR ν_{max}/cm⁻¹: 2924, 2855, 2361, 1651, 1519, 1489, 1443, 1335, 1273, 1173, 1065, 1018, 988, 949, 841, 764, 702.

Cuᴵᴵᴵ[Br₈TPC]. ¹H NMR: δ 7.63−7.67 (m, 2H), 7.39−7.53 (m, 13H). UV−vis: λ_{max} (log ϵ/(M⁻¹ cm⁻¹)) 441 nm (4.89), 641 nm (1.32). MS (MALDI-TOF): 1217.65 (M⁺); calcd 1218.33. IR ν_{max}/cm⁻¹: 3055, 3022, 2921, 2850, 2362, 2343, 1577, 1541, 1508, 1477, 1442, 1382, 1357, 1326, 1295, 1263, 1238, 1176, 1135, 1038, 1024, 1006, 938, 916, 872, 852, 839, 752, 739, 722, 694.

Cuᴵᴵᴵ[Br₈T(*p*-CF₃-P)C]. ¹H NMR: δ 7.73 (d, *J* = 8.6 Hz, 4H, *m*- or *o*-phenyl), 7.69 (d, *J* = 7.9 Hz, 2H, *m*- or *o*-phenyl), 7.64 (d, *J* = 7.9 Hz, 4H, *m*- or *o*-phenyl), 7.60 (d, *J* = 8.6 Hz, 2H, *m*- or *o*-phenyl). UV−vis: λ_{max} (log ϵ/(M⁻¹ cm⁻¹)) 434 nm (4.73). MS (MALDI-TOF): 1421.96 (M⁺); calcd 1422.33. IR ν_{max}/cm⁻¹: 2924, 2855, 2376, 1612, 1504, 1404, 1319, 1165, 1134, 1065, 1042, 1018, 880, 818, 733, 678.

Cuᴵᴵᴵ[Br₈T(*p*-OCH₃-P)C]. ¹H NMR: δ7.43−7.47 (m, 6H, *m*- or *o*-phenyl), 6.95−7.00 (m, 6H, *m*- or *o*-phenyl), 3.93 (s, 6H, *p*-OCH₃), 3.82 (s, 3H, *p*-OCH₃). UV−vis: λ_{max} (log ϵ/(M⁻¹ cm⁻¹)) 405 (4.54), 468 nm (4.81). MS (MALDI-TOF): 1307.27 (M⁺); calcd 1308.41. IR

ν_{max}/cm⁻¹: 2924, 2833, 2344, 1601, 1509, 1490, 1457, 1438, 1418, 1321, 1294, 1250, 1172, 1138, 1108, 1083, 1037, 1009, 950, 939, 870, 820, 805, 792, 744, 712, 668.

Cuᴵᴵᴵ[Br₈T(*p*-CH₃-P)C]. ¹H NMR: δ 7.42 (d, *J* = 6.4 Hz, 4H, *m*- or *o*-phenyl), 7.38 (d, *J* = 7.8 Hz, 2H, *m*- or *o*-phenyl), 7.26 (d, *J* = 6.8 Hz, 4H, *m*- or *o*-phenyl), 7.22 (d, *J* = 7.3 Hz, 2H, *m*- or *o*-phenyl), 2.44 (s, 6H, *p*-CH₃), 2.41 (s, 3H, *p*-CH₃). UV−vis: λ_{max} (log ϵ/(M⁻¹ cm⁻¹)) 453 nm (4.80). MS (MALDI-TOF): 1259.38 (M⁺); calcd 1260.41. IR ν_{max}/cm⁻¹: 2961, 2920, 2852, 2344, 1608, 1506, 1499, 1473, 1458, 1437, 1419, 1320, 1340, 1294, 1261, 1210, 1179, 1095, 1036, 1019, 939, 908, 869, 800, 705, 668.

Cuᴵᴵᴵ[Br₈TPFPC]. UV−vis: λ_{max} (log ϵ/(M⁻¹ cm⁻¹)) 442 (5.01), 596 nm (4.26). MS (MALDI-TOF): 1487.79 (M⁺); calcd 1488.02. IR ν_{max}/cm⁻¹: 2924, 2855, 2361, 1720, 1651, 1520, 1497, 1443, 1327, 1273, 1173, 1042, 980, 872, 787, 671. Preliminary UV−vis spectro-electrochemical studies in collaboration with Prof. Karl Kadish of the University of Houston suggest that in solution, this compound exists to a significant extent as [Cu(Br₈TPFPC)]⁻. Accordingly, the optical and resonance Raman spectra of [Cu(Br₈TPFPC)], shown in Figures 3 and 10, respectively, may actually correspond to the one-electron reduced derivative. This consideration does not apply to the other compounds studied in this paper. However, we believe that all the electrochemical potentials, including those of [Cu(Br₈TPFPC)], indicated in Table 1 are correctly assigned.

DFT Calculations. The ground-state and time-dependent DFT calculations were carried out with Slater-type valence triple-ζ plus polarization basis sets, the VWN local functional, the Perdew−Wang 1991 gradient corrections, a spin-restricted formalism, a fine mesh for numerical integration of matrix elements, full geometry optimizations, and the ADF program system. The theoretical methods used in ADF are discussed in refs 31 and 32. The ADF program system was obtained from Scientific Computing and Modeling, Department of Theoretical Chemistry, Vrije Universiteit, 1081 HV Amsterdam, The Netherlands. For details of basis sets, grids for numerical integration, etc., the reader is referred to the program manual obtainable from this source.

Results and Discussion

(a) Resonance Raman Spectroscopy. Our results in this area consist of the Soret-resonant Raman spectra of planar and nonplanar Cu(III) *meso*-triarylcorroles. The key conclusion is that the frequencies of a number of skeletal vibrations downshift significantly in the nonplanar corroles, relative to the planar analogues, in a manner that is exactly analogous to the behavior of RR marker bands of metalloporphyrins.[21] In other words, a number of the high-frequency RR bands of corroles serve as structure-sensitive marker bands.

Figure 3 depicts the Soret-resonant Raman spectra of the metallocorroles studied. The three high-frequency bands of Cuᴵᴵᴵ-[T(*p*-OCH₃-P)C] at 1403, 1488, and 1526 cm⁻¹, on β-octabromination of the corrole ligand, appear to downshift to 1388, 1459, and 1517 cm⁻¹, respectively. For Cuᴵᴵᴵ[T(*p*-CH₃-P)C], β-octabromination of the corrole ligand downshifts the high-frequency bands at 1404, 1487, and 1526 cm⁻¹ to 1393, 1460, and 1516 cm⁻¹, respectively. The marker bands of Cuᴵᴵᴵ[T(*p*-H-P)C] at 1406, 1488, 1499, 1516, and 1528 cm⁻¹ appear to downshift to 1387, 1462, 1495, 1506, and 1519 cm⁻¹, respectively, on β-octabromination. β-Octabromination of Cuᴵᴵᴵ[T(*p*-CF₃-P)C] downshifts the high-frequency marker bands at 1492, 1517, and 1529 cm⁻¹ to 1463, 1501, and 1522 cm⁻¹, respec-

(31) Velde, G. T.; Bickelhaupt, F. M.; Baerends, E. J.; Guerra, C. F.; Van Gisbergen, S. J. A.; Snijders, J. G.; Ziegler, T. *J. Comput. Chem.* **2001**, *22*, 931.
(32) van Gisbergen, S. J. A.; Snijders, J. G.; Baerends, E. J. *Comput. Phys. Commun.* **1999**, *118*, 119.
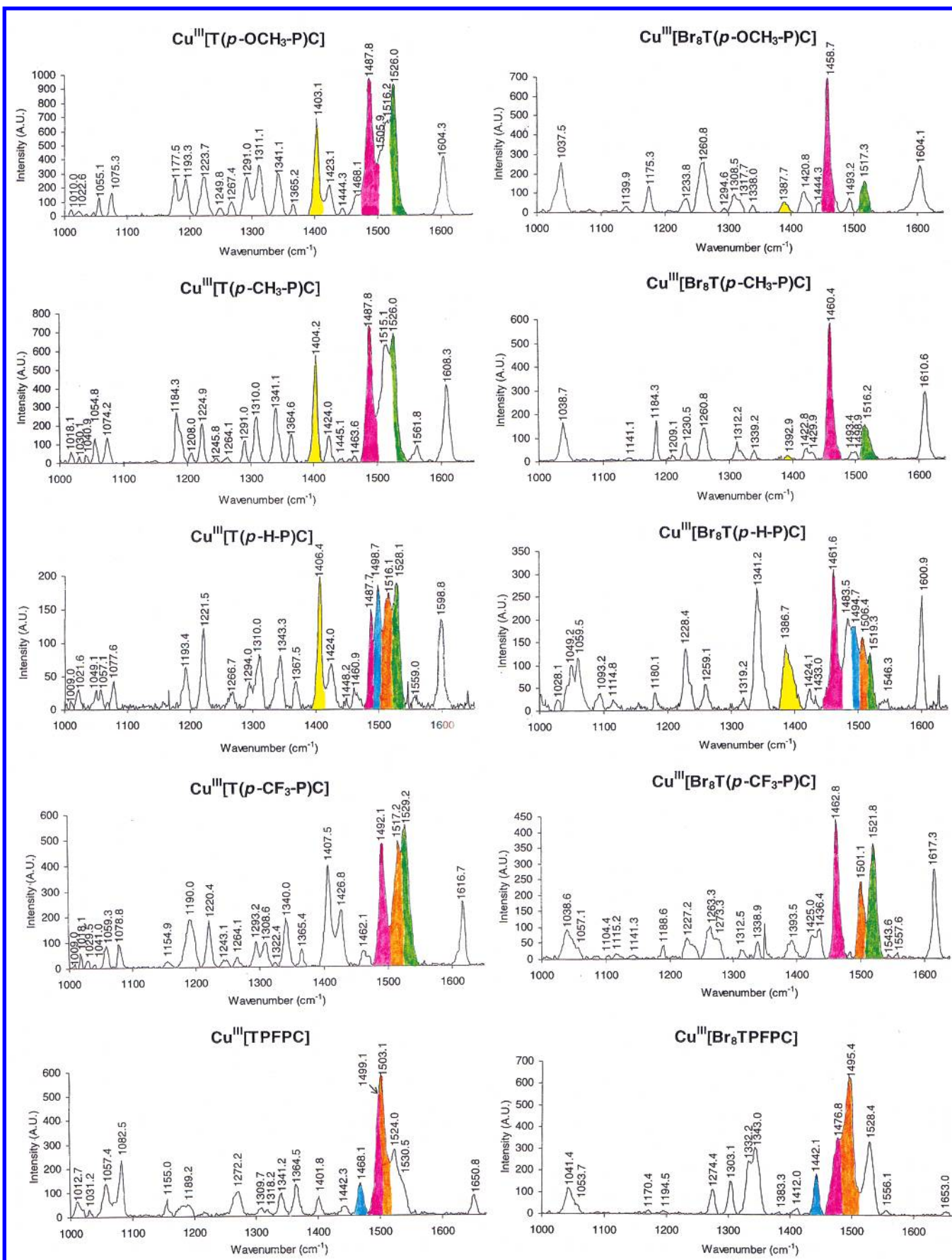
Figure 3. Resonance Raman spectra of Cu(III) triarylcorroles, with the marker bands indicated in color. The spectrum marked [Cu(Br₈TPFPC)] may actually be that of [Cu(Br₈TPFPC)]⁻. See experimental section for additional details.
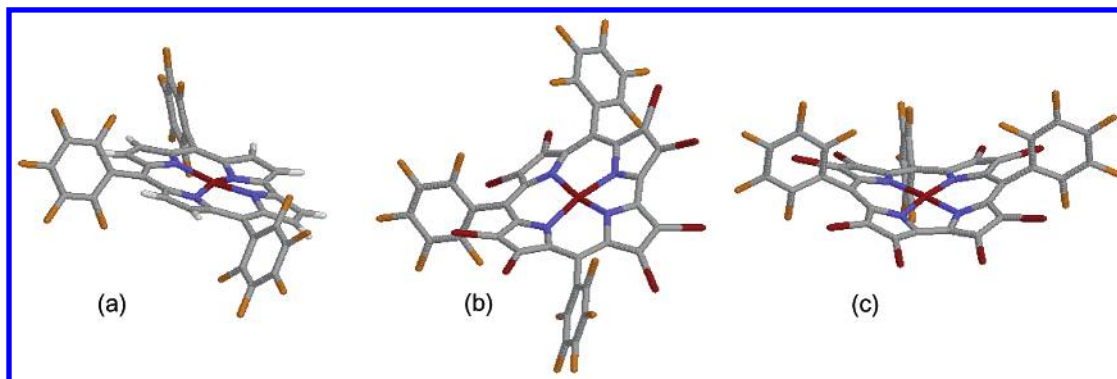
Figure 4. Stick diagrams of the optimized geometries of (a) Cu^{III}[TPFPC] and (b) saddled and (c) ruffled conformations of Cu^{III}[Br$_8$TPFPC].
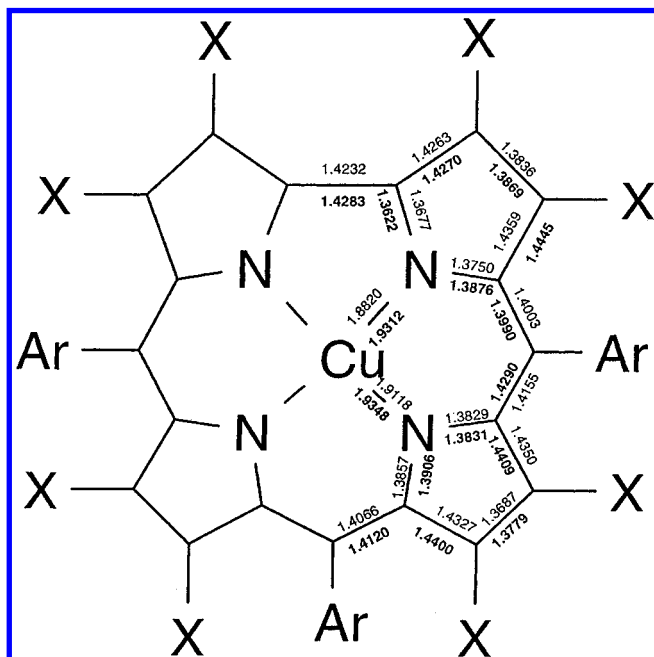
Figure 5. Selected optimized bond distances (Å) for Cu^{III}[TPFPC] (plain text) and the saddled conformation of Cu^{III}[Br$_8$TPFPC] (bold).

Table 1. Half-Wave Potentials, $E_{1/2}$ (V vs SCE), for Cu(III) Triarylcorroles in CH_2Cl_2 Containing 0.1 M TBAP and Hammett ρ Values (mV)

compd	p-X	3σ	Ox_1	Red_1	ρ_{ox}	ρ_{red}
Cu^{III}[T(p-X-P)C]	OCH$_3$	−0.80	0.65	−0.24	95	68
	CH$_3$	−0.51	0.70	−0.23		
	H	0	0.76	−0.20		
	CF$_3$	1.62	0.89	−0.08		
Cu^{III}[Br$_8$T(p-X-P)C]	OCH$_3$	−0.80	1.10	0.04	58	86
	CH$_3$	−0.51	1.12	0.07		
	H	0	1.14	0.12		
	CF$_3$	1.62	1.24	0.25		
Cu^{III}[TPFPC]			1.13	0.19		
Cu^{III}[Br$_8$TPFPC]			1.49	0.62		

tively. The high-frequency bands of Cu^{III}[TPFPC] (TPFPC = tris(pentafluorophenyl)corrole) at 1468, 1499, and 1503 cm^{-1}, on β-octabromination, appear to downshift to 1442, 1477, and 1495 cm^{-1}, respectively.

Although we have not yet accomplished vibrational analyses of the compounds studied in this work, we have carried out DFT(PW91/TZP) geometry optimizations of Cu^{III}[TPFPC] (C_2) and Cu^{III}[Br$_8$TPFPC]. Two optimizations were carried out for the latter compound, one for the C_2 saddled conformation (in which the pyrrole rings are alternately tilted above and below

the mean plane of the corrole) and one for the C_s ruffled conformation, and the results afford a qualitative understanding of the observed frequency downshifts in the nonplanar corrole derivatives.[33] The calculations clearly indicate the saddled conformation as the ground-state geometry of Cu^{III}[Br$_8$TPFPC], with the ruffled conformation about 0.7 eV higher in energy. The ruffled conformation may act as the transition state in the pseudorotational process of "saddling inversion" that connects the two enantiomeric saddled conformations of Cu^{III}[Br$_8$TPFPC]. Figure 4 presents stick diagrams of the various optimized geometries and Figure 5 depicts selected optimized skeletal bond distances for Cu^{III}[TPFPC] and the saddled conformation of Cu^{III}[Br$_8$TPFPC]. As shown in Figure 5, all C_β−C_β bonds, two symmetry-distinct C_α−C_{meso} bonds, and the Cu−N bonds undergo small, but significant expansions in Cu^{III}[Br$_8$TPFPC], relative to their lengths in Cu^{III}[TPFPC], which provides a qualitative rationale for the observed frequency downshifts for the nonplanar Cu(III) corrole derivatives studied. The frequency downshifts observed here parallel our observations on the effect of β-octahalogenation on the marker bands of metallotetraarylporphyrins. The porphyrin marker band frequencies ν_2 and ν_4 downshift across the series Ni^{II}[T(p-X-P)P] > Ni^{II}[Cl$_8$T(p-X-P)P] > Ni^{II}[Br$_8$T(p-X-P)P] for each para substituent X, where X = CH$_3$, H, F, CO$_2$Me, and NO$_2$, as well as across Cu^{II}[T(p-X-P)P] > Cu^{II}[Br$_8$T(p-X-P)P] (X = CH$_3$, H, F, CF$_3$, NO$_2$),[21] which suggests that the corrole marker bands described above may be crudely similar to the porphyrin ν_2 and ν_4 bands and, therefore, involve C_β−C_β and C_α−C_{meso} stretching.

Can the RR frequency downshifts observed for the β-octabrominated Cu(III) corroles be attributed to their nonplanar saddled conformation? Similarly, are the small but significant bond length expansions in Cu^{III}[Br$_8$TPFPC], relative to Cu^{III}-[TPFPC], directly attributable to nonplanarity? We believe that the answer to these questions is "no" because although all β-octabrominated porphyrins and corroles exhibit RR marker band frequency downshifts relative to their β-unbrominated analogues, not all β-octabromo-meso-triarylcorrole derivatives are appreciably nonplanar.[34,35] We propose that the RR frequency downshifts observed for the β-octabrominated corrole derivatives as well as the skeletal bond length expansions are a *direct* result of β-bromination rather than of nonplanarity of the corrole skeleton. Together with related results on porphyrins,[18−21] these results on corroles lead to a better understanding of the influence of nonplanar distortions on the vibrational

(33) For other DFT studies of porphyrin molecular structure, see: Ghosh, A. In *The Porphyrin Handbook*; Kadish, K. M., Guilard, R., Smith, K. M., Eds.; Academic Press: New York, 1999; Vol 7, pp 1−38.
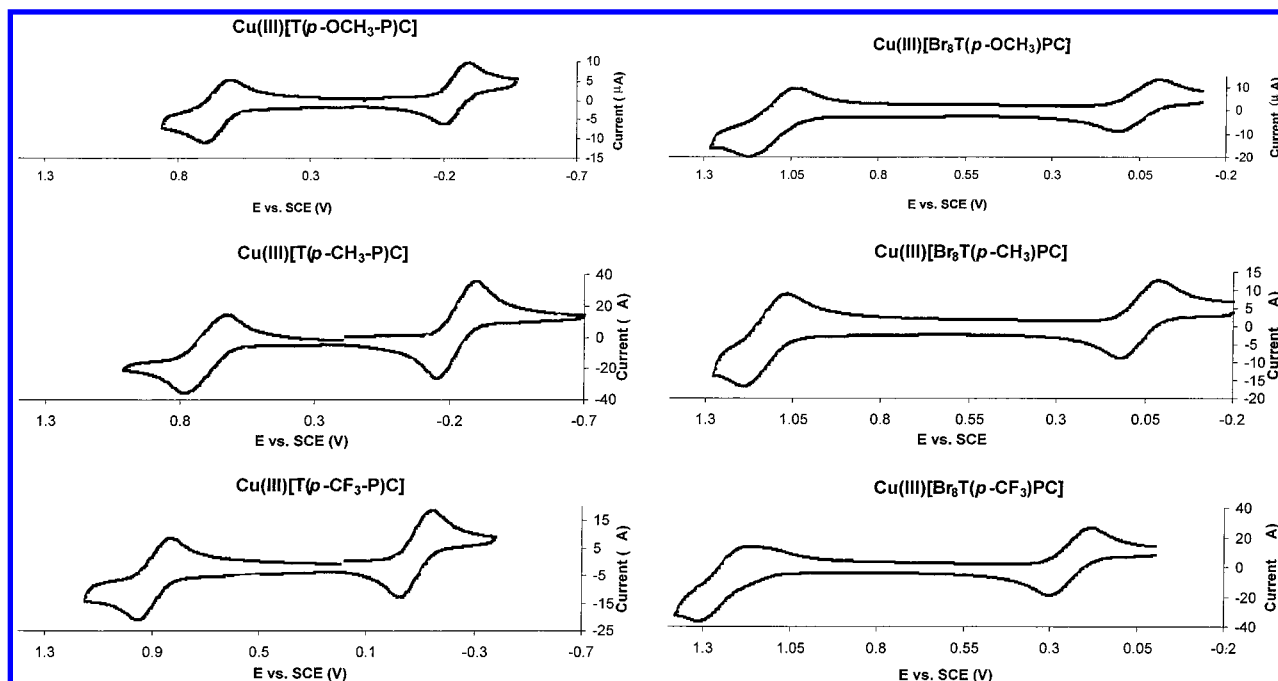
Figure 6. Selected cyclic voltammograms.

characteristics of tetrapyrroles and underscore the need for caution in ascribing shifts in vibrational frequencies to nonplanar distortions of the tetrapyrrole skeleton.

In another study,[36] we have reported that the high-frequency marker bands of corroles may also indicate potential radical character or noninnocence of the corrole ligand.[37] Three bands at 1470, 1523, and 1615 cm^{-1} of Mn^{III}[T(p-CF$_3$-P)C] upshift to 1486, 1528, and 1620 cm^{-1}, respectively, for Mn^{IV}[T(p-CF$_3$-P)C]Cl, consistent with partial π-cation radical character of the corrole ligand in the latter compound, a conclusion that was also supported by electrochemical measurements.[36]

Finally, the infrared spectra of the Cu(III) corroles (see Supporting Information) studied also exhibit some marker band behavior, though less clearly than the RR spectra. Thus, β-octabromination appears to downshift the IR bands of Cu^{III}-[TPC] at 1514, 1491, 1363, 1340, and 1309 cm^{-1} to 1508, 1477, 1357, 1326, and 1295 cm^{-1}, respectively. β-Octabromination appears to downshift the IR bands of Cu^{III}[T(p-CF$_3$-P)C] at 1520 and 1327 cm^{-1} to 1504 and 1319 cm^{-1}, respectively.

(b) Electrochemical Measurements. Table 1 presents the redox potentials (vs SCE) of the copper(III) corroles studied. Figure 6 presents representative cyclic voltammograms. The results lead to some of the first insights and generalizations related to substituent effects in metallocorroles. These are enumerated below.

(i) Substituents on the phenyl groups of planar Cu(III) *meso*-triarylcorroles exert a strong influence on the half-wave potential

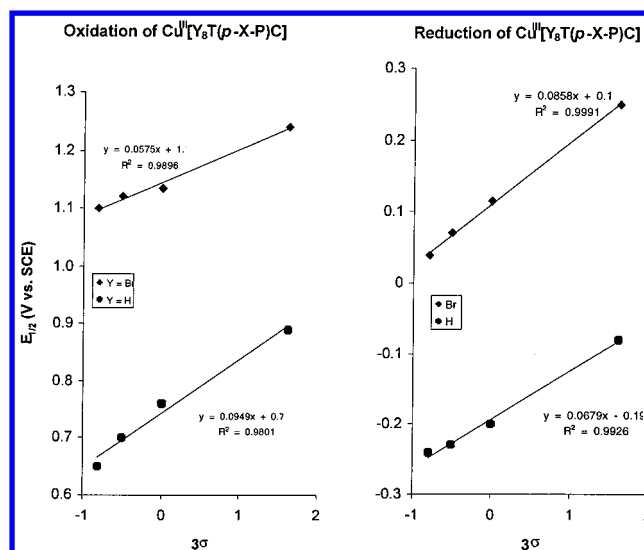(34) The crystal structure of (triphenylphosphine)(5,10,15-triphenyl-2,3,7,8,12, 13,17,18-octamethylcorrolato)cobalt(III) reported by Licoccia and co-workers (Paolesse, R.; Licoccia, S.; Bandoli, G.; Dolmella, A.; Boschi, T. *Inorg. Chem.* **1994**, *33*, 1171) exhibits a relatively planar macrocycle. However, the β-Br substituents in the brominated corrole derivatives we have studied are much more sterically demanding than methyl groups so the strongly saddled optimized geometry of Cu^{III}[Br$_8$TPFPC] is not unexpected.
(35) A crystal structure of (triphenylphosphine)(5,10,15-tris(p-nitrophenyl)-corrolato)cobalt(III) revealed a deviation from planarity of only 0.169 Å for the 23-atom corrole core (Paolesse, R.; Nardis, S.; Sagone, F.; Khoury, R. G. *J. Org. Chem.* **2001**, *66*, 550).
(36) Steene, E.; Wondimagegn, T.; Ghosh, A. *J. Inorg. Biochem.* **2002**, *88*, 113.
(37) Ghosh, A.; Steene, E. *J. Biol. Inorg. Chem.* **2001**, *7*, 739.

Figure 7. Hammett plots (Y = H or Br; X = OCH$_3$, CH$_3$, H, or CF$_3$).

for one-electron oxidation of these compounds. Thus, between X = OCH$_3$ and X = CF$_3$, the potential for one-electron oxidation of Cu^{III}[T(p-X-C$_6$H$_4$)C] increases by 240 mV. These large substituent effects, which translate into a Hammett ρ_{ox} [=$\Delta E_{1/2ox}/\Delta(3\sigma)$] of 95 mV (Figure 7 and Table 1), indicate removal of an electron from an MO that has large amplitudes at the meso positions. The corrole "b$_1$" HOMO satisfies this description (Figure 2).

(ii) A key feature of the compounds studied is that β-octabromination results in a dramatic increase in the half-wave potential for one-electron oxidation of Cu(III) triarylcorroles. For example, β-octabromination raises the half-wave potential for one-electron oxidation of Cu^{III}[T(p-OCH$_3$-C$_6$H$_4$)C] by 450 mV. In contrast, β-octabromination of Ni(II) tetraphenylpor-phyrin (Ni(TPP)) upshifts the half-wave potential for one-electron oxidation by only ~130 mV.[38] Similarly, β-octabro-mination of Zn(II) tetramesitylporphyrin (Zn(TMP)) leaves the potential for one-electron oxidation essentially unchanged![39]
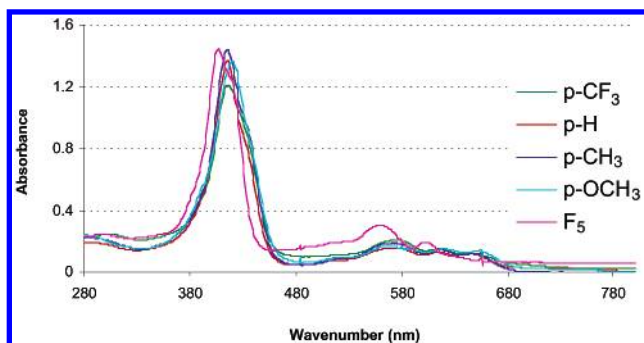
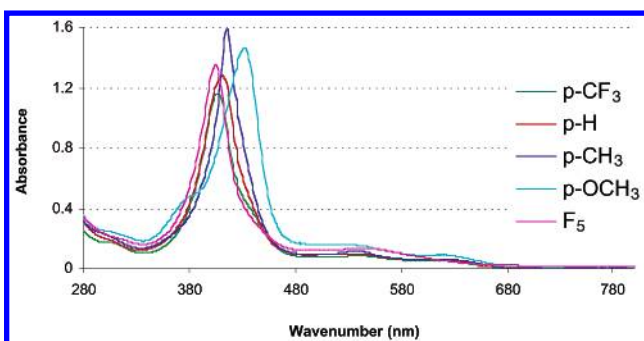**Figure 8.** Electronic absorption spectra of free-base corroles.

Figure 9. Electronic absorption spectra of Cu^{III} corroles.
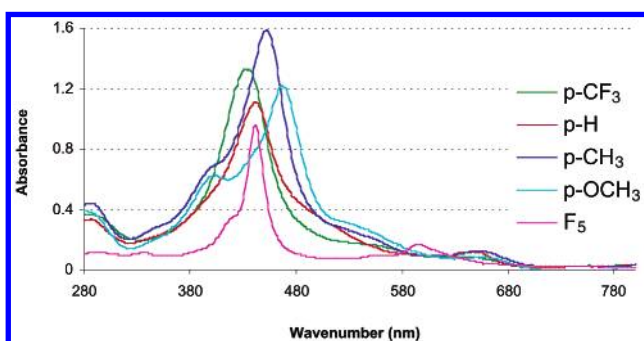

Figure 10. Electronic absorption spectra of Cu^{III}-β-octabromo corroles. The spectrum of $[Cu(Br_8TPFPC)]$ may actually be that of $[Cu(Br_8TPFPC)]^-$. See experimental section for additional details.

Table 2. Soret Band Absorption Maxima (nm) for *meso*-Triarylcorroles in Dichloromethane[a]

| | Ar = *p*-X-C$_6$H$_4$; X = | | | | Ar = |
corrole	OCH$_3$	CH$_3$	H	CF$_3$	C$_6$F$_5$
H$_3$[T(*p*-X-P)C]	421	417	417	417	408
Cu^{III}[T(*p*-X-P)C]	433	418	410	407	406
Cu^{III}[Br$_8$T(*p*-X-P)C]	468	453	441	434	
Fe^{IV}[T(*p*-X-P)C]Cl		361, **421**	359, **411**	366, **402**	
[Fe^{IV}T(*p*-X-P)C]$_2$O		389	385	384	
Mn^{IV}[T(*p*-X-P)C]Cl		319, 363, **443**	314, 358, **433**	316, 364, **423**	

[a]The free-base and Cu(III) results are from this work while the Fe and Mn corrole results are from ref 12. In the case of multiple Soret features, the highly substituent-sensitive bands are marked in bold.

Table 3. Valence Region of the (frozen-core) DFT Orbital Energy Spectrum of Ga(C)

irrep	serial no.	occupation	orbital energy (eV)
a$_1$	21	2.00	−9.65
a$_2$	3	2.00	−9.51
b$_2$	17	2.00	−9.49
a$_1$	22	2.00	−9.37
b$_2$	18	2.00	−9.26
a$_1$	23	2.00	−9.23
b$_2$	19	2.00	−9.19
b$_2$	20	2.00	−8.71
a$_1$	24	2.00	−8.63
b$_1$	4	2.00	−7.91
a$_2$	4	2.00	−6.85
b$_1$	5	2.00	−6.70
b$_1$	6	2.00	−6.68
b$_2$	21	2.00	−6.66
a$_2$	5	2.00	−6.22
b$_1$	7	2.00	−6.17
a$_2$	6	2.00	−5.92
a$_2$	**7**	**2.00**	**−4.82**
b$_1$	**8**	**2.00**	**−4.72**
a$_2$	**8**	**0.00**	**−2.79**
b$_1$	**9**	**0.00**	**−2.44**
b$_1$	10	0.00	−1.18
a$_1$	25	0.00	−0.39
b$_1$	11	0.00	−0.35
a$_2$	9	0.00	0.04
b$_1$	12	0.00	0.32
b$_2$	22	0.00	0.35
a$_1$	26	0.00	0.35
a$_1$	27	0.00	0.56
a$_2$	10	0.00	0.61
a$_1$	28	0.00	0.78
b$_2$	23	0.00	0.91

What accounts for this difference between corroles and porphyrins? In the case of porphyrins, the electron-withdrawing effect of the eight β-Br substituents is almost exactly balanced by the saddling-induced[40] destabilization of the porphyrin HOMOs. In the case of corroles, both the a$_2$ and b$_1$ HOMOs have significant to large amplitudes at the β-positions (unlike the a$_{2u}$ HOMO of porphyrins) and, therefore, the orbital energies of these MOs are strongly susceptible to the electronic effects of β-substituents.

(iii) Between Cu^{III}[T(*p*-OCH$_3$-C$_6$H$_4$)C] ($E_{1/2ox} = 0.65$ V) and Cu^{III}[Br$_8$TPFPC] ($E_{1/2ox} = 1.49$ V), the half-wave potentials for one-electron oxidation of the Cu(III) corroles studied span a range of 840 mV. Thus, although many metallocorroles are more easily oxidizable than analogous metalloporphyrins,[2] β-octabromo-*meso*-triarylmetallocorrole derivatives appear to be remarkably resistant toward oxidation and may find increasing application as stable catalysts or reagents under highly oxidizing reaction conditions.

(iv) Table 1 and Figure 7 show that the Hammett ρ for oxidation of planar Cu(III) triarylcorroles is much higher than that for oxidation of nonplanar Cu(III) β-octabromocorroles. These results are remarkably similar to those obtained for the nickel tetraphenylporphyrins, Ni[T(*p*-X-P)P] ($\rho_{ox} = 77$ mV) and Ni[Br$_8$T(*p*-X-P)P] ($\rho_{ox} = 27$ mV).[28] What accounts for this intriguing similarity between saddled porphyrins and corroles and how does saddling dampen substituent effects on the half-wave potential for one-electron oxidation? A simple explanation that accounts for these observations involves an a$_{1u}$/a$_{2u}$ or a$_2$/b$_1$

(38) Kadish, K. M. In *The Porphyrin Handbook*; Kadish, K. M., Smith, K. M., Guilard, R., Eds.; Academic: San Diego, CA, 2000; Vol. 9, Chapter 59, p 1.
(39) Ochsenbein, P.; Ayougou, K.; Mandon, D.; Fischer, J.; Weiss, R.; Austin, R. N.; Jayaraj, K.; Gold, A.; Terner, J.; Fajer, J. *J. Angew. Chem., Int. Ed. Engl.* **1994**, *33*, 348.
(40) Ryeng, H.; Ghosh, A. *J. Am. Chem. Soc.* **2002**, *124*, 8099. In this paper, we present a reevaluation of whether ruffling and saddling really destabilize the HOMOs of tetrapyrroles. Theoretical studies suggest that the destabilization of the HOMOs is better described as resulting from changes in skeletal bond distances and angles brought about by peripheral substituents, the same substituents that also bring about the nonplanar distortions. However, in this paper, we shall not discuss this subtle issue any further.

            Wasbotten et al.

Table 4. Transition Energies (<4 eV), Oscillator Strengths, and MO → MO Composition of the Singlet−Singlet Transitions of Ga(C)

(a) The A₁ Transitions

no.	transition energy (eV)	oscillator strength	no.	transition energy (eV)	oscillator strength
1 (Q)	**2.35**	**0.16×10^{-1}**	6	3.90	0.77×10^{-2}
2 (B)	**3.21**	**0.26**	7	4.34	0.13×10^{-2}
3 (B)	**3.38**	**0.39**	8	4.40	0.15×10^{-1}
4	3.60	0.28×10^{-1}	9	4.47	0.37×10^{-1}
5	3.68	0.12×10^{-5}	10	4.78	0.60×10^{-4}

major excitation contributions in the above A₁ transitions

transition	nature of excitation	% contribution	transition	nature of excitation	% contribution
1 (Q)	**7a2 → 8a2**	**59**	7	5b1 → 9b1	30
1 (Q)	**8b1 → 9b1**	**39**	7	6b1 → 9b1	5
2 (B)	**6a2 → 8a2**	**52**	8	6b1 → 9b1	86
2 (B)	**8b1 → 9b1**	**26**	8	5b1 → 9b1	5
2 (B)	**7a2 → 8a2**	**18**	9	8b1 → 11b1	67
3 (B)	**6a2 → 8a2**	**45**	9	5b1 → 9b1	15
3 (B)	**8b1 → 9b1**	**29**	9	4a2 → 8a2	9
3 (B)	**7a2 → 8a2**	**17**	10	5b1 → 9b1	29
4	5a2 → 8a2	95	10	7a2 → 9a2	23
5	8b1 → 10b1	91	10	8b1 → 11b1	23
6	7b1 → 9b1	92	10	4a2 → 8a2	11
7	4a2 → 8a2	57	10	6b1 → 9b1	4

(b) The A₂ Transitions (note zero oscillator strength)

no.	excitation energy (eV)	oscillator strength	no.	excitation energy (eV)	oscillator strength
1	4.26571	0.000	2	4.43526	0.000

major excitation contributions in the above A₂ transitions

transition	nature of excitation	% contribution	transition	nature of excitation	% contribution
1	21b2 → 9b1	100	2	7a2 → 25a1	100

(c) The B₁ Transitions (note zero oscillator strength)

no.	excitation energy (eV)	oscillator strength	no.	excitation energy (eV)	oscillator strength
1	3.84889	0.000	2	4.26822	0.000

major excitation contributions in the above B1 transitions

transition	nature of excitation	% contribution	transition	nature of excitation	% contribution
1	21b2 → 8a2	100	2	8b1 → 25a1	100

(d) The B₂ Transitions

no.	excitation energy (eV)	oscillator strength	no.	excitation energy (eV)	oscillator strength
1 (Q)	**2.36**	**0.28×10^{-1}**	**7 (L)**	**4.08**	**0.64×10^{-1}**
2 (B)	**3.17**	**0.48**	8	4.23	0.32×10^{-1}
3	3.52	0.64×10^{-5}	9	4.54	0.78×10^{-2}
4 (N)	**3.65**	**0.88×10^{-1}**	10	4.73	0.49×10^{-1}
5	3.74	0.26×10^{-2}	11	4.89	0.11
6	3.95	0.12×10^{-2}			

major excitation contributions in the above B₂ transitions

transition	nature of excitation	% contribution	transition	nature of excitation	% contribution
1 (Q)	**8b1 → 8a2**	**65**	8	5b1 → 8a2	71
1 (Q)	**7a2 → 9b1**	**32**	8	5a2 → 9b1	8
2 (B)	**7a2 → 9b1**	**59**	8	8b1 → 9a2	06
2 (B)	**8b1 → 8a2**	**28**	8	7a2 → 11b1	5
2 (B)	**6a2 → 9b1**	**4**	9	4a2 → 9b1	67
3	7b1 → 8a2	81	9	7a2 → 11b1	23
3	6a2 → 9b1	16	10	7a2 → 11b1	40
4	6a2 → 9b1	76	10	6a2 → 10b1	39
4	7b1 → 8a2	15	10	4a2 → 9b1	7
5	7a2 → 10b1	89	10	8b1 → 9a2	7
6	5a2 → 9b1	66	11	6a2 → 10b1	41
6	6b1 → 8a2	25	11	8b1 → 9a2	34
7	6b1 → 8a2	70	11	7a2 → 11b1	11
7	5a2 → 9b1	21	11	5a2 → 10b1	9

HOMO reversal in the case of the saddled d⁸ metallotetrapyrroles. For saddled d⁸ metallotetrapyrroles, a bonding interaction between the "a₂ᵤ" (D_{4h} notation for metalloporphyrins) or "b₁" (C_{2v} notation for metallocorroles) ligand HOMO and the metal $d_{x^2-y^2}$ MO becomes symmetry-allowed and, accordingly, saddling preferentially stabilizes the "a₂ᵤ" or "b₁" HOMO relative

to the "a$_{1u}$" or "a$_2$" HOMO.[28] Thus, for the series of saddled corroles studied, it is no longer certain that the HOMO is b$_1$. In terms of irreducible representations of the C_{2v} point group, it is indeed likely that the HOMO is a$_2$ for a number of saddled corrole derivatives studied. The corrole a$_2$ HOMO has relatively little amplitude at the *meso* positions, which is consistent with the small substituent effects observed for oxidation of the saddled corroles.

(v) We have not yet characterized the one-electron oxidized and reduced products of the Cu(III) corroles. Various spectro-electrochemical studies of the different Cu(III) corroles are in progress. However, Kadish et al. have furnished EPR evidence that Cu(III) corroles undergo metal-centered reductions, yielding Cu(II) corroles.[41] As in the case of the Cu(III) corroles described here, Boschi, Kadish, and co-workers[13] have reported a relatively large ρ value of 92 mV for reduction of their Co(III) corrole derivatives. However, they considered this value rather large for metal-centered (i.e. Co(III)/Co(II)) reduction. The present results suggest that such large ρ values may well be possible for metal-centered reductions of corrole derivatives.

(vi) Finally, it is instructive to compare the half-wave potentials for one-electron oxidation of the Cu(III) corroles studied here with those of other transition metal corroles. The main point that emerges from such a comparison is that for a particular corrole ligand, the potentials for one-electron oxidation of the Cu^{III}, Sn^{IV}Ph, and Fe^{IV}Ph (and Fe^{IV}OFe^{IV}) complexes are generally significantly lower than those of the Sn^{IV}Cl, Fe^{IV}-Cl, Mn^{IV}Cl, and Cr^V(O) complexes.[2,26,37] For example, for the triphenylcorrole (TPC) ligand, the half-wave potential for one-electron oxidation of the Cu(III) complex is 0.64 V, compared with 1.07 and 1.03 V for the Fe^{IV}Cl and Mn^{IV}Cl complexes, respectively. This appears to be a relatively simple consequence of the greater electron-withdrawing power (or electronegativity) of the Sn^{IV}Cl, Fe^{IV}Cl, Mn^{IV}Cl, and Cr^V(O) ions relative to the Cu^{III} Sn^{IV}Ph and Fe^{IV}Ph ions. Elsewhere,[12] we have expressed the same idea in somewhat "fancier" language, saying that the relatively high half-wave potentials for one-electron oxidation of Fe(IV)Cl and Mn(IV)Cl corrole complexes reflect the fact the corrole ligand in these complexes is already partially oxidized (i.e. noninnocent) and has some radical character. Thus, the electronic structure of Fe(IV)Cl and Mn(IV)Cl corrole complexes may be described, at least to a significant degree, as involving antiferromagnetic coupling between a corrole radical and an Fe(III) ($S = {}^3/_2$) or Mn(III) ($S = 2$) center. This description was first proposed by Walker and co-workers for (octaalkylcorrolato)Fe^{IV}Cl derivatives on the basis of NMR studies.[9] Our own DFT calculations provided significant support for this picture.[12,36,37] Interestingly, for the highly electron-deficient tris(pentafluorophenyl)corrole (TPFPC) ligand, the half-wave potential for one-electron oxidation of the Cu(III) complex is 1.13 V, which is essentially comparable with potentials of 1.20, 1.24, and 1.24 V for the Sn^{IV}Cl, Fe^{IV}Cl, and Cr^V(O) complexes, respectively.[2,26,37] In other words, there seems to be relatively little difference in electronic character between the TPFPC ligand in the Cu(III) complex on one hand and the Sn^{IV}Cl, Fe^{IV}Cl, and Cr^V(O) complexes on the other hand. In turn, this may indicate that the TPFPC ligand in the Sn^{IV}Cl, Fe^{IV}Cl, and Cr^V(O) complexes has relatively little radical

Table 5. The (frozen-core) DFT Orbital Energy Spectrum of Cu(C)

irrep	serial no.	occupation	orbital energy (eV)
a$_1$	21	2.00	−9.85
a$_1$	22	2.00	−9.63
a$_2$	2	2.00	−9.55
b$_2$	18	2.00	−9.36
a$_1$	23	2.00	−9.31
b$_2$	19	2.00	−9.24
b$_2$	20	2.00	−9.11
a$_1$	24	2.00	−8.86
b$_1$	4	2.00	−8.71
a$_2$	3	2.00	−8.69
b$_2$	21	2.00	−8.36
a$_1$	25	2.00	−8.15
a$_1$	26	2.00	−7.96
b$_1$	5	2.00	−7.95
a$_2$	4	2.00	−6.85
b$_1$	6	2.00	−6.71
b$_1$	7	2.00	−6.56
a$_2$	5	2.00	−6.09
b$_1$	8	2.00	−5.98
a$_2$	6	2.00	−5.88
a$_2$	**7**	**2.00**	**−4.76**
b$_1$	**9**	**2.00**	**−4.63**
b$_2$	**22**	**0.00**	**−4.52 (Cu d$_{x^2-y^2}$)**
a$_2$	**8**	**0.00**	**−2.72**
b$_1$	**10**	**0.00**	**−2.32**
b$_1$	11	0.00	−0.72
a$_1$	27	0.00	0.08
a$_2$	9	0.00	0.13
b$_1$	12	0.00	0.38
b$_2$	23	0.00	0.46
a$_1$	28	0.00	0.50
a$_2$	10	0.00	0.67
a$_1$	29	0.00	0.76
a$_1$	30	0.00	0.91
b$_1$	13	0.00	0.92

character, i.e., is relatively innocent, and correspondingly, the metal is more "truly" high-valent in the TPFPC complexes than in complexes with more electron-rich corrole ligands such as TPC.[42]

(c) Electronic Absorption Spectroscopy. Electrochemical measurements of redox potentials provide perhaps the most convenient means of probing substituent effects for many classes of compounds,[38,43] photoelectron spectroscopy[44,45] and measurements of electron affinities[46] being some of the additional methods suitable for this purpose. In contrast, as mentioned above, optical spectroscopy is far less generally useful in this regard because substituents often tend to shift the HOMO and LUMO energy levels to comparable degrees so that substituent effects on the excitation energies of molecules are often minimal. The optical spectra of the Cu(III) triarylcorroles studied constitute a striking deviation from this generalization.

Figures 8−10 present the optical spectra of (1) the free-base triarylcorrole ligands, H$_3$TArC, (2) their Cu(III) complexes, Cu^{III}[TArC], and (3) the β-octabrominated Cu(III) complexes, Cu^{III}[Br$_8$TArC]. Table 2 lists the Soret absorption maxima for all compounds. Note that for the free-base corroles, the Soret

(41) Kadish, K. M.; Adamian, V. A.; Van Caemelbecke, E.; Gueletii, E.; Will, S.; Erben, C.; Vogel, E. *J. Am. Chem. Soc.* **1998**, *120*, 11986.

(42) Tangen, E.; Ghosh, A. *J. Am. Chem. Soc.* **2002**, *124*, 8117. Theoretical calculations suggest that the corrolazine ligand in metallocorrolazines is typically more innocent than the corrole ligand in metallocorroles.
(43) Kadish, K. M. *Prog. Inorg. Chem.* **1986**, 435.
(44) Gassman, P. G.; Ghosh, A.; Almlöf, J. *J. Am. Chem. Soc.* **1992**, *114*, 9990.
(45) Ghosh, A. *J. Am. Chem. Soc.* **1995**, *117*, 4691.
(46) Chen H. L.; Ellis P. E.; Wijesekera T.; Hagan, T. E.; Groh, S. E.; Lyons, J. E.; Ridge, D. P. *J. Am. Chem. Soc.* **1994**, *116*, 1086.

Table 6. Transition Energies (<4 eV), Oscillator Strengths, and MO → MO Composition of the Singlet−Singlet Transitions of Cu(C)[a]

(a) The A_1 Transitions

no.	excitation energy (eV)	oscillator strength	no.	excitation energy (eV)	oscillator strength
1 (Q)	**2.37**	**0.21×10^{-1}**	6	4.04	0.35×10^{-2}
2 (B)	**3.07**	**0.29**	7	4.37	0.22×10^{-1}
3 (L)	**3.36**	**0.67×10^{-1}**	8	4.44	0.35×10^{-2}
4	3.52	0.12×10^{-1}	9	4.54	0.16
5	3.82	0.55×10^{-3}			

major excitation contributions in the above A_1 transitions

transition	nature of excitation	% contribution	transition	nature of excitation	% contribution
1	**$7a_2 \rightarrow 8a_2$**	**63**	6	$21b_2 \rightarrow 22b_2$	5
1	**$9b_1 \rightarrow 10b_1$**	**35**	7	$7b_1 \rightarrow 10b_1$	85
2	**$9b_1 \rightarrow 10b_1$**	**49**	7	$4a_2 \rightarrow 8a_2$	8
2	**$7a_2 \rightarrow 8a_2$**	**26**	8	$4a_2 \rightarrow 8a_2$	54
2	**$6a_2 \rightarrow 8a_2$**	**12**	8	$6b_1 \rightarrow 10b_1$	29
2	**$21b_2 \rightarrow 22b_2$**	**10 (LMCT)**	8	$7b_1 \rightarrow 10b_1$	7
3	**$6a_2 \rightarrow 8a_2$**	**85**	9	$20b_2 \rightarrow 22b_2$	46 (LMCT)
3	**$9b_1 \rightarrow 10b_1$**	**5**	9	$21b_2 \rightarrow 22b_2$	30 (LMCT)
4	$5a_2 \rightarrow 8a_2$	6	9	$18b_2 \rightarrow 22b_2$	7 (LMCT)
5	$8b_1 \rightarrow 10b_1$	92	9	$9b_1 \rightarrow 12b_1$	3
6	$9b_1 \rightarrow 11b_1$	79	9	$6b_1 \rightarrow 10b_1$	2
6	$4a_2 \rightarrow 8a_2$	9			

(b) The A_2 Transitions (note zero oscillator strength)

no.	excitation energy (eV)	oscillator strength	no.	excitation energy (eV)	oscillator strength
1	0.14	0.000	4	2.19	0.000
2	1.57	0.000	5	3.43	0.000
3	2.09	0.000	6	4.59	0.000

major excitation contributions in the above A_2 transitions

transition	nature of excitation	% contribution	transition	nature of excitation	% contribution
1	$9b_1 \rightarrow 22b_2$	100	4	$6b_1 \rightarrow 22b_2$	100
2	$8b_1 \rightarrow 22b_2$	100	5	$5b_1 \rightarrow 22b_2$	100
3	$7b_1 \rightarrow 22b_2$	100	6	$4b_1 \rightarrow 22b_2$	99

(c) The B_1 Transitions (note zero oscillator strength)

no.	excitation energy (eV)	oscillator strength	no.	excitation energy (eV)	oscillator strength
1	0.25	0.93×10^{-6}	4	2.33	0.44×10^{-6}
2	1.46	0.26×10^{-4}	5	4.56	0.38×10^{-5}
3	1.65	0.83×10^{-4}			

major excitation contributions in the above B_1 transitions

transition	nature of excitation	% contribution	transition	nature of excitation	% contribution
1	$7a2 \rightarrow 22b2$	100	4	$4a2 \rightarrow 22b2$	100
2	$6a2 \rightarrow 22b2$	99	5	$3a2 \rightarrow 22b2$	98
3	$5a2 \rightarrow 22b2$	99			

(d) The B_2 Transitions

no.	excitation energy (eV)	oscillator strength	no.	excitation energy (eV)	oscillator strength
1 (Q)	**2.36**	**0.36×10^{-1}**	6	4.01	0.14×10^{-1}
2 (B)	**3.04**	**0.26**	7	4.04	0.11×10^{-1}
3	3.39	0.85×10^{-3}	8	4.08	0.79×10^{-2}
4	3.69	0.24×10^{-1}	9	4.26	0.12
5	3.92	0.20×10^{-1}	10	4.44	0.28×10^{-2}

major excitation contributions in the above B_2 transitions

transition	nature of excitation	% contribution	transition	nature of excitation	% contribution
1	**$9b_1 \rightarrow 8a_2$**	**73**	7	$6a_2 \rightarrow 10b_1$	6
1	**$7a_2 \rightarrow 10b_1$**	**24**	8	$7a_2 \rightarrow 11b_1$	41
2	**$7a_2 \rightarrow 10b_1$**	**65**	8	$6b_1 \rightarrow 8a_2$	27
2	**$9b_1 \rightarrow 8a_2$**	**18**	8	$25a_1 \rightarrow 22b_2$	25 LMCT
2	**$25a_1 \rightarrow 22b_2$**	**11 (LMCT)**	**9**	**$24a_1 \rightarrow 22b_2$**	**32 (LMCT)**
3	$8b_1 \rightarrow 8a_2$	97	**9**	**$6b_1 \rightarrow 8a_2$**	**24**
4	$6a_2 \rightarrow 10b_1$	87	**9**	**$25a_1 \rightarrow 22b_2$**	**22 (LMCT)**
4	$7b_1 \rightarrow 8a_2$	5	**9**	**$9b_1 \rightarrow 9a_2$**	**6**
5	$5a_2 \rightarrow 10b_1$	85	**9**	**$5a_2 \rightarrow 10b_1$**	**4**
5	$7b_1 \rightarrow 8a_2$	5	10	$7a_2 \rightarrow 11b_1$	29
6	**$7b_1 \rightarrow 8a_2$**	**68**	10	$6b_1 \rightarrow 8a_2$	27
6	**$26a_1 \rightarrow 22b_2$**	**23 (LMCT)**	10	$24a_1 \rightarrow 22b_2$	17 LMCT
7	**$26a_1 \rightarrow 22b_2$**	**66 (LMCT)**	10	$4a_2 \rightarrow 10b_1$	13
7	**$7b_1 \rightarrow 8a_2$**	**18**	10	$9b_1 \rightarrow 9a_2$	6

[a] Note that the B bands have significant LMCT character as do some higher-energy transitions. Some of the more notable features of the data are indicated in bold.

absorption maxima are rather insensitive to substituent effects. In sharp contrast, on going from $Cu^{III}[T(p\text{-}CF_3\text{-}P)C]$ to Cu^{III}-$[T(p\text{-}OCH_3\text{-}P)C]$, the Soret maximum red shifts by 26 nm, from 407 to 433 nm. Similarly, on going from $Cu^{III}[Br_8T(p\text{-}CF_3\text{-}P)C]$ to $Cu^{III}[Br_8T(p\text{-}OCH_3\text{-}P)C]$, the Soret absorption red shifts by 34 nm, from 434 to 468 nm. A plausible explanation for these dramatic substituent effects is that one or more transitions in the composite Soret band have significant ligand-to-metal charge transfer (LMCT) character.[47]

To investigate the likelihood of this explanation, we have carried out time-dependent density functional theoretical calculations on unsubstituted gallium(III) corrole [Ga(C)] and copper(III) corrole [Cu(C)].[24] Table 3 shows that the orbital energy spectrum of Ga(C) corresponds to Gouterman's four-orbital model, i.e., the two HOMOs are near-degenerate as are the two LUMOs and these four MOs are well-separated energetically from all other occupied and virtual MOs. Table 4 correctly reproduces the expected energies and relative oscillator strengths of the Q- and B-bands. As has been found for other nontransition-metal porphyrins,[48,49] the Q-bands have nearly pure four-orbital character whereas the B-bands have some significant "non-four-orbital" $\pi-\pi^*$ character.

The orbital energy spectrum of Cu(C), shown in Table 5, is significantly different, relative to Ga(C), the key feature being that the LUMO of Cu(C) is a σ MO (22 b_2 in Table 5), which has largely Cu $d_{x^2-y^2}$ character. The Q-bands of Cu(C) still have standard "four-orbital" character (Table 6). But the two B/Soret transitions, of A_1 and B_2 symmetry, at 3.0–3.1 eV have about 10–11% LMCT character (Table 6), confirming our hypothesis based on the experimentally observed substituent effects on the Soret absorption maximum. We speculate that with a larger triarylcorrole ligand, transitions in the Soret region may acquire even more enhanced LMCT character.

Elsewhere,[12] we have reported that the Soret bands of other high-valent triarylcorroles such as Fe(IV)Cl, Mn(IV)Cl, and dimeric Fe(IV)-O-Fe(IV) corrole derivatives are also highly sensitive to substituents on the *meso*-phenyl groups (Table 2). This, then, appears to be an important spectroscopic feature common to high-valent metallocorroles and presumably also to other high-valent metallotetrapyrroles but not to free-base or non-high-valent derivatives. Thus, the Soret absorption maxima of non-high-valent (5,10,15-tri-X-phenyl-2,3,7,8,12,13,17,18-octamethylcorrolato)cobalt(III) triphenylphosphine complexes (where X = *p*-OCH₃, *p*-CH₃, *p*-Cl, *m*-Cl, *o*-Cl, *m*-F, *o*-F, or H) are not substituent-sensitive but are remarkably constant at 380 ± 2 nm.[13] Whether the existence of LMCT states of Cu(III) and other transition metal corroles are indicative of other interesting properties, e.g. nonlinear optical properties such as large first-order hyperpolarizabilities, β, remains to be seen.

Conclusions

We have presented an analysis of substituent effects in two series of (planar and nonplanar) Cu(III) triarylcorroles. As is often the case, the various measurements of substituent effects

have also served as powerful probes of broader electronic-structural issues such as the geometric and electronic consequences of nonplanar distortions of the tetrapyrrole skeleton and the nature of high-valent transition metal complexes and of ligand noninnocence. The findings on the optical spectra of high-valent transition metal corroles are also an important contribution, in our opinion, to the already rich field of electronic absorption spectroscopy of tetrapyrroles and their complexes. The main conclusions of this study may be summarized as follows:

(1) We have synthesized a number of free-base *meso*-triarylcorroles with different para substituents on the aryl groups using the procedure reported by Gross for the synthesis of H₃-TPFPC. We have found the Gross procedure to be more general than originally claimed! It works for the synthesis of triarylcorroles with *either* electron-rich *or* electron-deficient aryl groups. The copper(III) complexes of the various triarylcorroles prepared were also readily accessible and β-octabromination of the copper(III) derivatives also went smoothly.

(2) DFT calculations indicated that the saddled conformation should be significantly preferred over the ruffled conformation for the fully substituted copper(III) β-octabromo *meso*-triarylcorroles, consistent with crystallographic studies of related compounds.

(3) The RR (and IR) results show that at least two and possibly more high-frequency bands in the 1400–1550 cm⁻¹ region exhibit significant frequency downshifts on β-octabromination and, thus, qualify as structure-sensitive marker bands. Interestingly, we have argued that these downshifts are *not* a direct result of saddling of the corrole skeleton. We believe that an extensive systematics of structure–frequency correlations, similar to what is available for porphyrins, will also emerge for metallocorroles within the foreseeable future.

(4) The electrochemical results on substituent effects in metallocorroles reveal some significant similarities and differences between metallocorroles and metalloporphyrins. The results underscore the importance of the metal($d_{x^2-y^2}$)–corrole-(b_1)/porphyrin(a_{2u}) orbital interaction as a critical determinant of the electronic properties of d⁸ metalloporphyrins and metallocorroles. Another significant finding is that although many metallocorroles are much more easily oxidizable than analogous metalloporphyrins, β-octahalogeno-*meso*-triarylcorrole derivatives may prove to be extremely rugged catalysts or reagents under highly oxidizing conditions.

(5) A comparison of the half-wave potentials for one-electron oxidation of different metallocorroles has revealed that for a particular corrole ligand, the half-wave potentials for one-electron oxidation of the Cu^{III} $Sn^{IV}Ph$ and $Fe^{IV}Ph$ (and Fe^{IV}-OFe^{IV}) complexes are significantly lower than those of the $Sn^{IV}Cl$, $Fe^{IV}Cl$, $Mn^{IV}Cl$, and $Cr^V(O)$ complexes, suggesting that the corrole ligands in the former complexes are more innocent, relative to the latter complexes. In other words, electrochemical potentials appear to provide an effective probe — in addition to NMR and other magnetic resonance studies — of the nature of the corrole ligand in metallocorroles.

(6) Finally, the Soret absorption maxima of high-valent metallotriarylcorroles exhibit a striking dependence on the substituents on the *meso*-aryl groups. Time-dependent DFT calculations suggest that this substituent dependence is indicative of significant ligand-to-metal charge transfer character of certain

(47) LMCT transitions are responsible for the special features of the optical spectra of hyperporphyrins. For a recent study, see: Vitasovic, M.; Gouterman, M.; Linschitz, H. *J. Porphyrins Phthalocyanines* **2001**, *5*, 191.

(48) Parusel, A. B. J.; Ghosh, A. *J. Phys. Chem. A* **2000**, *104*, 2504 and references therein.

(49) See e.g.: Rosa, A.; Ricciardi, G.; Baerends, E. J.; van Gisbergen, S. J. A. *J. Phys. Chem. A* **2001**, *105*, 3311 and references therein.

transitions in the Soret region. We believe that the optical spectra of the compounds studied here, along with those of Fe(IV) and Mn(IV) corroles we have described elsewhere, provide some of the "cleanest" examples of substituent effects on LMCT transitions in high-valent transition metal complexes. The optical spectra of free-base and non-high-valent metallotetrapyrroles, in general, do not exhibit a similar, readily observable substituent dependence.

Supporting Information Available: ^{1}H NMR and IR spectra of the new compounds and infrared spectra of the Cu(III) corroles (PDF). This material is available free of charge via the Internet at http://pubs.acs.org.

JA0113697